Maximum likelihood-based method for angular differential imaging

L. M. Mugnier[a,c], A. Cornia[a,b,c], J.-F. Sauvage[a,c], N. Védrenne[a,c], T. Fusco[a,c] and G. Rousset[b,c].

[a] ONERA/DOTA, B.P. 72, 92322 Châtillon cedex, France.
[b] LESIA, Observatoire de Paris, 5 place Jules Janssen, 92195 Meudon, France.
[c] Groupement d'Intérêt Scientifique PHASE (Partenariat Haute résolution Angulaire Sol Espace) between ONERA, Observatoire de Paris, CNRS and Université Paris Diderot.

ABSTRACT

In the context of the SPHERE planet finder project, we further develop a recently proposed method, based on detection theory, for the efficient detection of planets using angular differential imaging.

The proposed method uses the fact that with the SPHERE instrument the field rotates during the night, and can additionally use the fact that at each acquisition time, two images are recorded by the IRDIS instrument in two different spectral channel.

The method starts with the appropriate combination of images recorded at different times, and potentially in different spectral channels, into so-called pseudo-data. It then uses jointly all these pseudo-data in a Maximum-Likelihood (ML) framework to detect the position and amplitude of potential companions of the observed star, taking into account the mixture of photon and detector noises and a positivity constraint on the planet's amplitude. A reasonable detection criterion is also proposed; it is based on the computation of the noise propagation from the images to the estimated flux of the potential planet. The method is validated on data simulating realistic conditions of operation, including residual aberrations before and after the coronagraph, residual turbulence after adaptive optics correction, and noise.

Keywords: exoplanets, detection, inverse problems, coronagraphy, angular imaging, differential imaging, maximum likelihood, adaptive optics.

1. INTRODUCTION

The direct detection of exoplanets from the ground is a very promising field of astronomy today. The light emitted by exoplanet is related to the composition of their atmosphere. This detection from the ground is a technological challenge, since the contrast between the star and its companion is no less than 10^6 in IR bands. The European project SPHERE[1–3] is the planet searcher of VLT (ESO), based on direct imaging in the near-IR. The goal of SPHERE is to detect warm Jupiters, orbiting sun-like stars at $10pc$ from the Sun. These planets present atmosphere rich in methane, and present therefore interesting spectral signatures around 1.6 µm. The planets are searched for at a few diffraction elements (λ/D) from their parent star.

The SPHERE instrument is the combination between several optical features, all of them optimized toward the final goal, which is exoplanet detection. First of all, the extreme adaptive optics system (XAO) concentrates the light into a coherent Airy pattern, performing a real-time correction of atmospheric turbulence. The optical quality is a key factor in direct exoplanet detection, since the main limitation of faint objects is demonstrated to be the residual speckles in images. These speckles are the consequence of an imperfect correction of statics aberrations. Then, the coronagraphic stage allows to deeply attenuate the star flux. The photons are physically removed, allowing the reduction of the photon noise in the final image. The considered coronagraphs in the SPHERE project are a Lyot coronagraph,[4] a Four Quadrant Phase Mask (FQPM)[5] and an apodized Lyot coronagraph (APLC).[6]

Further author information: send correspondence to L.M.M.: Laurent (dot) Mugnier (at) onera (dot) fr

The combination of XAO and coronagraphic device is necessary to reduce both speckle and photon noise in the final image, but is not sufficient. Indeed, the contrast between the star and the planet at 1.6 µm is close to 10^6. In order to reach the ultimate detection performance needed to detect a warm Jupiter, it is mandatory to combine the abovementioned optical devices to an *a posteriori* processing of all data.

The main problematic is to disentangle the potential companion's signal from the quasi static speckles, which are due to residual aberrations and constitute a major "noise" source. These speckles present the same characteristic angular size as the diffraction element, λ/D, and the same size as the companion's signal. With no more information, it is impossible to discriminate between the speckles and the companion. In order to do so, the SPHERE instrument includes the ability to perform spectral and angular differential imaging.

Spectral differential imaging consists in acquiring simultaneous images of the system star-companion at different wavelengths. The spectral signatures of the exoplanet's atmosphere ensures that the planet's response will significantly vary in the images, while the star response and therefore the speckles remain the same. With the IRDIS instrument[7] of SPHERE, we can make use of two spectral channels, *e.g.*, between bands $H2 = 1.59$ µm and H3=1.64 µm.

Angular differential imaging is a method originally designed for the calibration of residual static speckle of the Hubble Space Telescope.[8] The idea was to perform a rotation of the entire telescope, and therefore of the observed field on the detector, whereas the static speckles would remain the same. This idea has been developed recently in the case of a ground based observation,[9] where the field rotates naturally as the instrument follows the object in the sky with a stabilized pupil. In an image series obtained in these conditions, the additional information we have at hand is therefore the expected trajectory of the companion in the numerous "temporal channels" of the series.

If both temporal and spectral channels are available, as is the case with the SPHERE instrument, then one may first combine each pair of simultaneous spectral images into one image so as to enhance the planet's signal, and then use the resulting image series as temporal channels for angular imaging.

In this paper, we investigate the joint processing of such temporal series of images.

2. ADOPTED APPROACH FOR ANGULAR DIFFERENTIAL IMAGING

At least two approaches are possible for this problem:

- jointly estimate the coronagraphic response of the star, and the companion's position and amplitude (or flux). This approach has been adopted by Smith *et al.*;[10]
- numerically remove the star signal, and only estimate the planet.[11,12]

In the framework of the SPHERE project, the static aberrations are likely to evolve during observing time, and the estimation of the star signal should therefore be done several times during night. We therefore choose the second option, which consists in cancelling the star image numerically.

This suppression is done by a pairwise subtraction of sufficiently separated images, as illustrated in Figure 1. Let $\boldsymbol{i}_t$ the raw images, the new data are the images differences $\Delta(\boldsymbol{r}, k) \triangleq \boldsymbol{i}_{k_1(k)}(\boldsymbol{r}) - \boldsymbol{i}_{k_2(k)}(\boldsymbol{r})$, where $k_1(k)$ and $k_2(k)$ are indices chosen so as to preserve the planet's signal in the difference. The estimation of the companion's position and amplitude is done on these new data, through a Maximum Likelihood approach.

3. MAXIMUM LIKELIHOOD ESTIMATION FOR POSITION AND AMPLITUDE OF THE COMPANION

In the new data consisting of the $k_{\max}$ differential images denoted by $\Delta(\boldsymbol{r}, k)$, and assuming that a planet is indeed present, the data model at each pixel $\boldsymbol{r}$ of image k is the following:

$$\Delta(\boldsymbol{r}, k) = a.\boldsymbol{p}(\boldsymbol{r}, k; \boldsymbol{r}_0) + \boldsymbol{n}(\boldsymbol{r}, k), \tag{1}$$

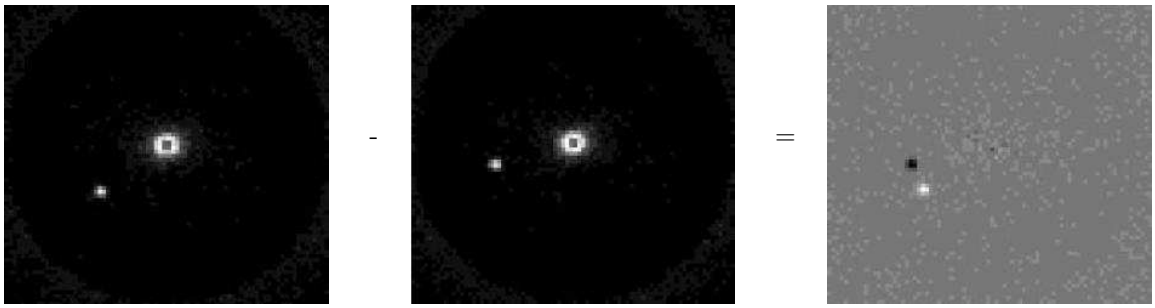

Figure 1. Left and center: two raw coronagraphic images of a star with a bright companion. Right: difference, canceling completely the star response in this case where the quasi-static aberrations have not evolved.

where a is the planet's amplitude and $\boldsymbol{r}_0$ is the initial planet's position, $\boldsymbol{p}(\boldsymbol{r}, k; \boldsymbol{r}_0)$ is the known pattern of the planet in this data for an assumed $\boldsymbol{r}_0$ (which is the difference of two PSF's), and $\boldsymbol{n}(\boldsymbol{r}, k)$ denotes the noise.

The maximum likelihood approach consists in searching for $(\hat{\boldsymbol{r}}_0, \hat{a})$ that maximize the likelihood $L(\boldsymbol{r}_0, a)$. In the following we assume that the noise is non-homogeneous, Gaussian and white, with variance $\sigma^2(\boldsymbol{r}, k)$. This assumption is reasonable and allows us to take into account both the photon and the detector noises, as done in AO-corrected image restoration:[13] for the flux levels considered here, the Poisson statistics of photon noise is well approximated by a Gaussian probability density, and its variance map can be estimated from the set of images, *e.g.*, as an empirical variance of the image series at each pixel. As to the detector read-out noise, it is reasonably homogeneous white Gaussian and its variance can be estimated beforehand.

The likelihood is given by:

$$L(\boldsymbol{r}_0, a) \propto \exp\left\{-\frac{1}{2}\sum_k \sum_{\boldsymbol{r}} \frac{\left|\Delta(\boldsymbol{r}, k) - a\, p(\boldsymbol{r}, k; \boldsymbol{r}_0)\right|^2}{2\sigma^2(\boldsymbol{r}, k)}\right\} \tag{2}$$

Maximizing this likelihood with respect to $(\boldsymbol{r}_0, a)$ is equivalent to maximizing the following metric, which is equal to the log-likelihood up to unimportant constants:

$$J(\boldsymbol{r}_0, a) = 2 \ln L(\boldsymbol{r}_0, a) + \text{const} = -a^2 \sum_{k,\boldsymbol{r}} \frac{p^2(\boldsymbol{r}, k; \boldsymbol{r}_0)}{\sigma^2(\boldsymbol{r}, k)} + 2a \sum_{k,\boldsymbol{r}} \frac{p(\boldsymbol{r}, k; \boldsymbol{r}_0)\Delta(\boldsymbol{r}, k)}{\sigma^2(\boldsymbol{r}, k)} \tag{3}$$

The optimal value $\hat{a}(\boldsymbol{r}_0)$ of a for each given $\boldsymbol{r}_0$ is computable analytically:

$$\hat{a}(\boldsymbol{r}_0) = \frac{\sum_{k,\boldsymbol{r}} p(\boldsymbol{r}, k; \boldsymbol{r}_0)\Delta(\boldsymbol{r}, k)/\sigma^2(\boldsymbol{r}, k)}{\sum_{k,\boldsymbol{r}} p^2(\boldsymbol{r}, k; \boldsymbol{r}_0)/\sigma^2(\boldsymbol{r}, k)} \tag{4}$$

The numerator of this expression can be seen as a scalar product (correlation) between the planet's patterns and the images, with weights given by the noise variance. And the denominator is simply a normalization constant.

If we insert this optimal value for the amplitude into metric J, we obtain an expression of the latter that depends, explicitly at least, only on the sought planet position:

$$J'(\boldsymbol{r}_0) \triangleq J(\boldsymbol{r}_0, \hat{a}(\boldsymbol{r}_0)) = \frac{\left(\sum_{k,\boldsymbol{r}} p(\boldsymbol{r}, k; \boldsymbol{r}_0)\Delta(\boldsymbol{r}, k)/\sigma^2(\boldsymbol{r}, k)\right)^2}{\sum_{k,\boldsymbol{r}} p^2(\boldsymbol{r}, k; \boldsymbol{r}_0)/\sigma^2(\boldsymbol{r}, k)}. \tag{5}$$

This criterion J' can be computed for each possible initial planet position on a grid, which can be chosen as the original pixel grid of the images, or as a finer grid if it is useful. The most likely initial planet's position is then $\hat{\boldsymbol{r}}_0 = \arg\min J'(\boldsymbol{r}_0)$, and the most likely amplitude is $\hat{a}(\hat{\boldsymbol{r}}_0)$ as computed with Eq. (4).

This estimator can be improved by constraining the estimated amplitude to be positive. Indeed, the value of $\hat{a}(\boldsymbol{r}_0)$ of Eq. (4) is not necessarily positive, whereas the true amplitude is. Additionally, because the estimation of $\hat{a}(\boldsymbol{r}_0)$ is a one-dimensional optimization, the optimal amplitude subject to the positivity constraint is simply:

$$\hat{a}_{\text{pos}}(\boldsymbol{r}_0) = \max\{\hat{a}(\boldsymbol{r}_0), 0\}. \tag{6}$$

If we now insert this value for the planet's amplitude into metric J, it is easy to show that we obtain

$$J"(\boldsymbol{r}_0) \triangleq J(\boldsymbol{r}_0, \hat{a}_{\text{pos}}(\boldsymbol{r}_0)) = \begin{cases} J'(\boldsymbol{r}_0) & \text{if } \hat{a}(\boldsymbol{r}_0) > 0 \\ 0 & \text{if } \hat{a}(\boldsymbol{r}_0) \leq 0, \end{cases} \tag{7}$$

where $J'(\boldsymbol{r}_0)$ is given by Eq. (5), $\hat{a}(\boldsymbol{r}_0)$ by Eq. (4). Note that because the numerator of J' of Eq. (5) is the square of that of $\hat{a}(\boldsymbol{r}_0)$ of Eq. (4), $J"$ in the above equation is very different from a thresholded version of J' and has less local maxima.

Figures 2 and 3 illustrates the usefulness of the positivity constraint in the case of a bright companion. Figure 2 shows the map of the estimated companion's amplitude without (left) and with (right) the positivity constraint. In the case without positivity the map is very similar to the autocorrelation of the planet pattern, which explains its shape with two negative bumps. Figure 3 shows the corresponding map of the log-likelihood obtained without (Equation (5)) and with (Equation (7)) the positivity constraint on the amplitude. Clearly, the positivity constraint removes the sidelobes of the log-likelihood and hence should contribute to removing false detections in a noisier case.

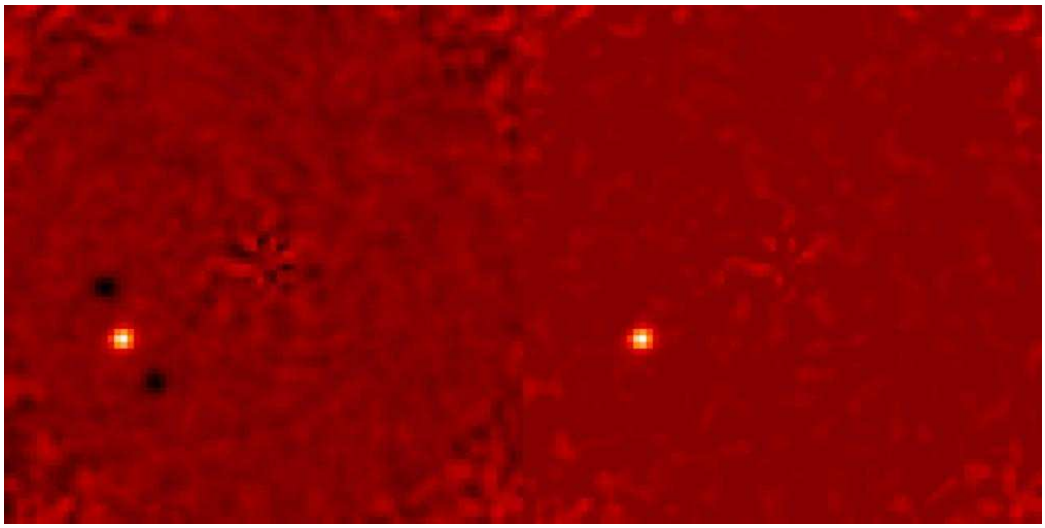

Figure 2. Map of a bright companion's amplitude estimated without (left) and with (right) the positivity constraint.

4. DETECTION CRITERION

Once the likelihood and amplitude maps are computed, the main problem is to decide which peaks are true companions and which ones are not. One way to do so is to additionally compute the standard deviation of the estimated amplitude, $\sigma(\hat{a}(\boldsymbol{r}_0))$, for each possible planet position $\boldsymbol{r}_0$, *i.e.*, to compute how the noise propagates from the images to our amplitude estimator. A possible detection criterion, which can be linked to the probability of false alarm, is then to decide that all positions where the signal-to-noise ratio (SNR) of the estimated amplitude, defined as:

$$\text{SNR}(a) \triangleq \hat{a}(\boldsymbol{r}_0)/\sigma(\hat{a}(\boldsymbol{r}_0)), \tag{8}$$

is greater than some threshold are true detections.

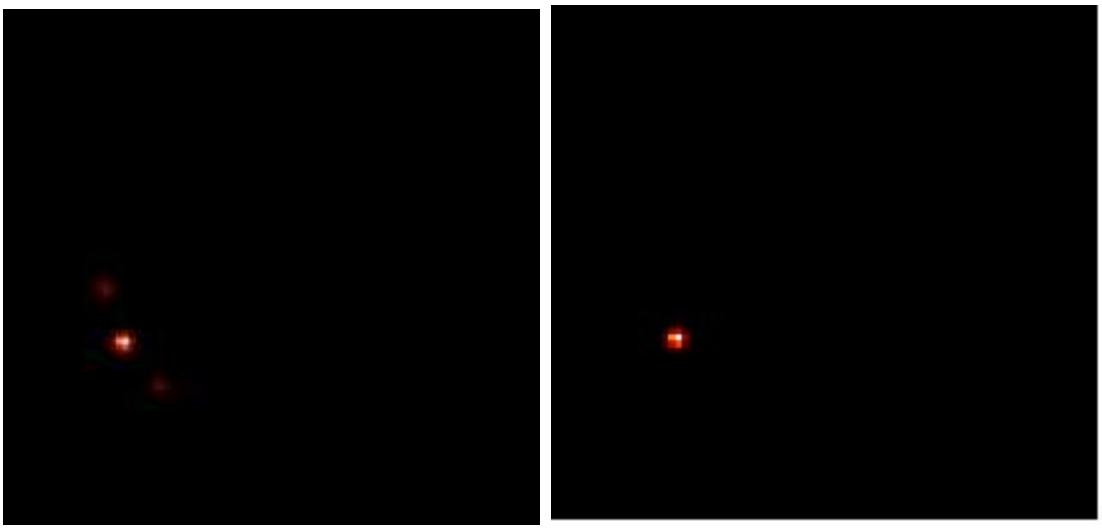

Figure 3. Log-likelihood of the position of the bright companion of Fig. 2 without (left) and with (right) the positivity constraint in the estimation of the flux.

The variance of the estimated flux for a given position $\boldsymbol{r}_0$ is computed by means of Eq. (4) using the fact that the noise in our images $\Delta(k, \boldsymbol{r})$ is white, both temporally and spatially:

$$\sigma^2(\hat{a}(\boldsymbol{r}_0)) = \frac{1}{\left(\sum_{\boldsymbol{r}',k'} \frac{p^2(\boldsymbol{r}',k';\boldsymbol{r}_0)}{\sigma^2(\boldsymbol{r}',k')}\right)^2} \times \sum_{\boldsymbol{r},k} \left(\frac{p(\boldsymbol{r},k;\boldsymbol{r}_0)}{\sigma^2(\boldsymbol{r},k)}\right)^2 \times \sigma^2(\boldsymbol{r},k),$$

which can be simplified into:

$$\sigma^2(\hat{a}(\boldsymbol{r}_0)) = \left(\sum_{\boldsymbol{r},k} \frac{p^2(\boldsymbol{r},k;\boldsymbol{r}_0)}{\sigma^2(\boldsymbol{r},k)}\right)^{-1}. \tag{9}$$

Interestingly, the SNR of the estimated amplitude is linked very directly to the log-likelihood J' of Eq. (5):

$$J'(\boldsymbol{r}_0) = \left[\hat{a}(\boldsymbol{r}_0)/\sigma(\hat{a}(\boldsymbol{r}_0))\right]^2 = \left[\mathrm{SNR}(a)\right]^2. \tag{10}$$

Consequently, maximizing (or thresholding) the likelihood is actually equivalent to maximizing (respectively thresholding) the SNR of the estimated amplitude.

5. VALIDATION BY SIMULATION

5.1 Simulation conditions

The conditions of simulation are representative of the SPHERE/IRDIS instrument on the VLT:

- an 8 m telescope, a seeing of $0.8''$, a wind speed of 12.5 m/s;
- a SAXO-like AO system: 41×41 actuators, a 40×40 sub-aperture Hartmann-Shack wavefront sensor, a sampling frequency of 1200 Hz;
- residual static aberrations with a standard deviation of $\sigma_{\phi_u} = 35$ nm upstream of the coronagraph and $\sigma_{\phi_d} = 100$ nm downstream of the coronagraph. We have assumed a pupil-stabilized mode, with residual aberrations kept constant during the simulated run.

A hundred 256×256 images are simulated at an imaging wavelength of $\lambda = 1.593\ \mu$m with Poisson (photon) noise. The image of the star is computed by means of the analytical expression for the long-exposure AO-corrected coronagraphic image of a star.[14]

We have simulated seven planets which lie aligned at distances multiple of $4\lambda/D$ from the central star. The long-exposure AO-corrected images of the planets are computed using the static aberrations and the residual phase structure function, assuming that the planets do not "see" the coronagraph.

The star flux is $2.67 \cdot 10^7$ ph/s, the planet flux is 28.5 ph/s, which yields a ratio of $9.36 \cdot 10^5$. Depending on the simulation, the total exposure time is either 1h or 2h. For the purpose of the validation of our method, we have simulated the field rotation in the following simplified way:

- the step between two consecutive images is constant (for 100 images it is 1°);
- the angle between the first and the last image is 120°; the parallactic angles of the star are centered on the meridian and there is a gap of $\sim 20°$ around the meridian, to prevent the overlapping of the planet signals of two images that are to be subtracted.

The image combination scheme we chose is to associate each image with its symmetrical one with respect to the meridian (the first image with the last, the second with the last-but-one, etc.).

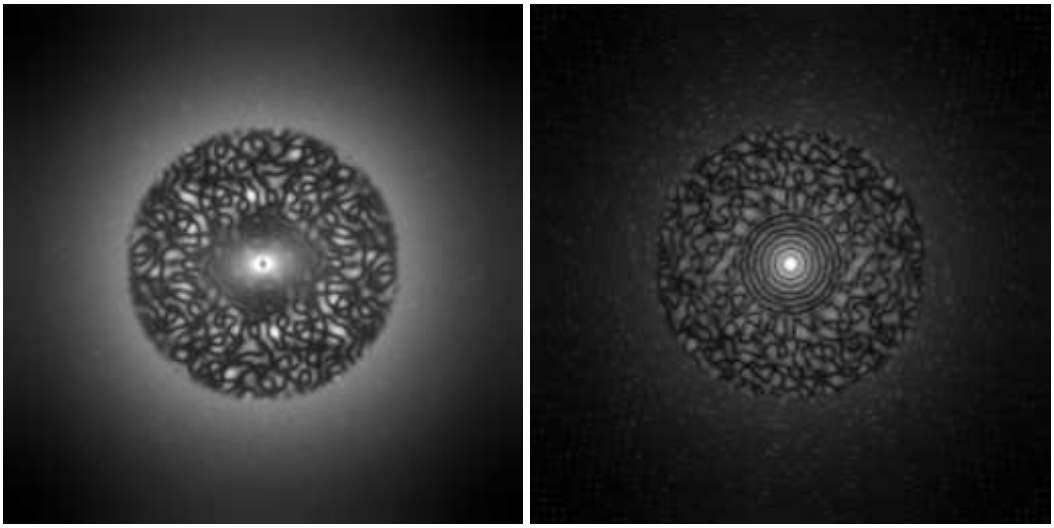

Figure 4. Simulated PSFs with (left) and without (right) coronagraph, in logarithmic scale. The former one is used for the star, the latter one for the planet after proper positioning. Note that for legibility each of these two images is represented with its own gray-level scale (with white corresponding to its maximum value).

5.2 Impact of the proposed positivity constraint and of the noise variance map

Both the positivity constraint on the planet's amplitude and the use of a (non-homogeneous) noise variance map correspond to taking into account additional prior knowledge: if the noise variance map is unknown, one will use a homogeneous (*i.e.*, constant) noise variance map, which cancels out in all above expressions. As shown in Fig. 5, this prior knowledge does improve the likelihood map and thus the detection: going from the homogeneous noise variance without positivity (top-left) to the homogeneous noise variance with positivity (top-right) notably decreases low-level peaks of the likelihood as well as some high-level peaks that correspond to false alarms (for instance one in the middle, below the center of the image). These are the peaks due to the negative values of the estimated amplitude.

Additionally, going then from the homogeneous noise variance with positivity (top-right) to the inhomogeneous noise variance with positivity (bottom-right) further improves the likelihood map by dimming some other spurious peaks (for instance one on the top-left part of the image, at about 45° from the star).

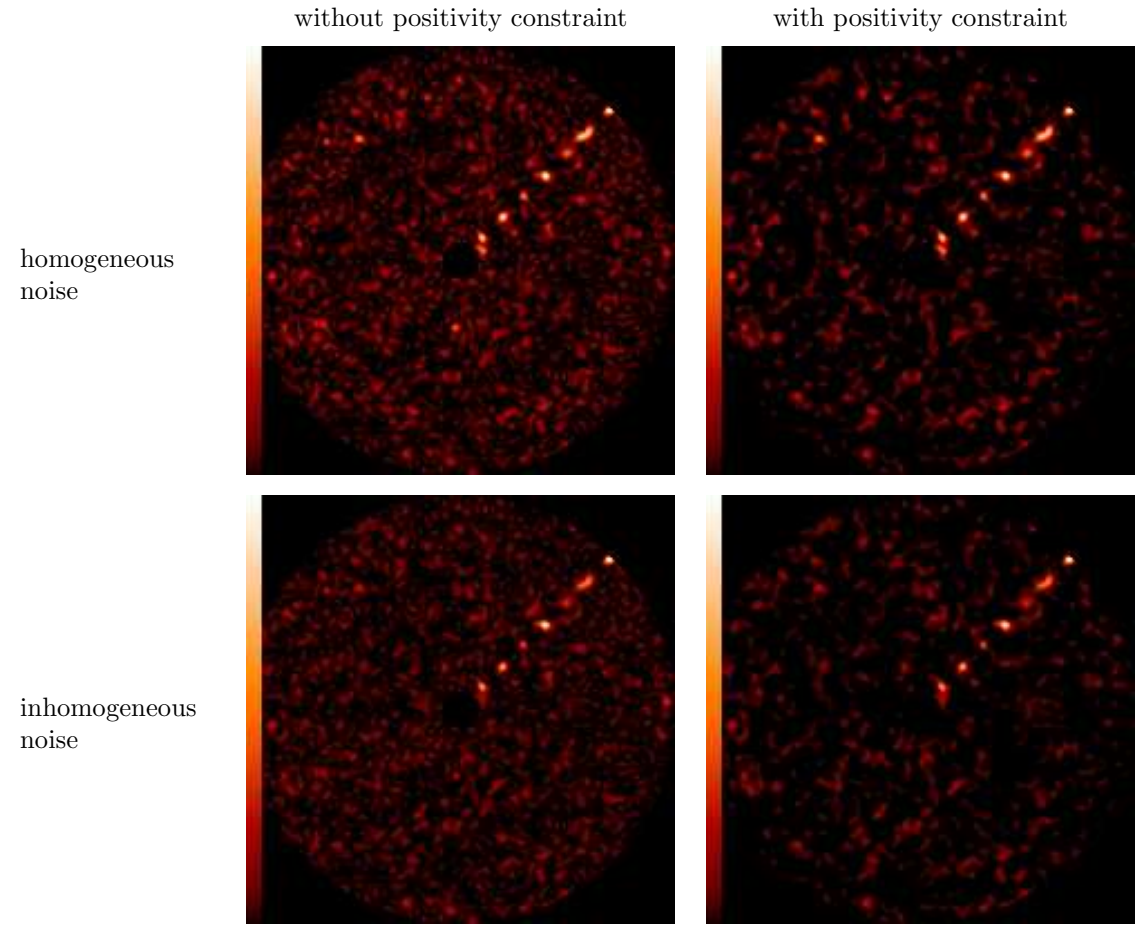

Figure 5. Likelihood maps with 100 images and an exposure time of 1 h. Top row: homogeneous noise. Bottom row: inhomogeneous noise. Left column: without positivity constraint. Right column: with positivity constraint.

In order to better quantify the improvement brought by positivity and by the use of an inhomogeneous noise variance map, Fig. 6 shows the SNR of the estimated amplitude (defined by Equation (8)) thresholded to values from 3 to 6, in the difficult case of a one hour total observation time. In the two cases where a homogeneous noise is assumed in the processing, the noise variance has been taken equal to the spatial average of the empirical variance of each pixel in time.

For the case where both the positivity and the inhomogeneous noise variance map are used, there exists, in this simulation, a threshold (of 4) for which all the true planets are detected and no false alarm is present. The corresponding detection map is the boxed one of Fig. 6. For the three other cases, whatever the chosen threshold, in this simulation there are either false alarms (for low threshold values) or undetected planets (for high threshold values).

5.3 Impact of the exposure time

Fig. 7 illustrates the influence of the exposure time on the likelihood maps and on the detection maps for several threshold values. As expected, for two hours of total exposure time instead of one, (1) there are less false detections for low thresholds (3 standard deviations, second line of the figure), and (2) all planets are detected even for higher threshold values (up to 5 standard deviations, last line of the figure).

6. CONCLUSION

We presented a method based on maximum likelihood for exoplanet detection with ground-based instruments such as SPHERE, and validated it by realistic simulations. This method makes use of the temporal diversity of the images brought by field rotation in order to disentangle planets from speckles. It may be easily applied to bi-spectral images. It can enforce a positivity constraint on the estimated flux and can use the noise variance map of the images, the beneficial influence of which has been demonstrated. A reasonable detection criterion has also been proposed and tested; it is based on the computation of the noise propagation from the images to the estimated flux of the potential planet. Perspectives include assessing the performance of the method in the case of slowly evolving aberrations.

ACKNOWLEDGMENTS

The authors thank David Mouillet (LAOG) for sharing his expertise on the SPHERE system, and many people from the SPHERE consortium for several fruitful discussions, notably Marcel Carbillet, Anthony Boccaletti, Maud Langlois, Kjetil Dohlen and Jean-Luc Beuzit.

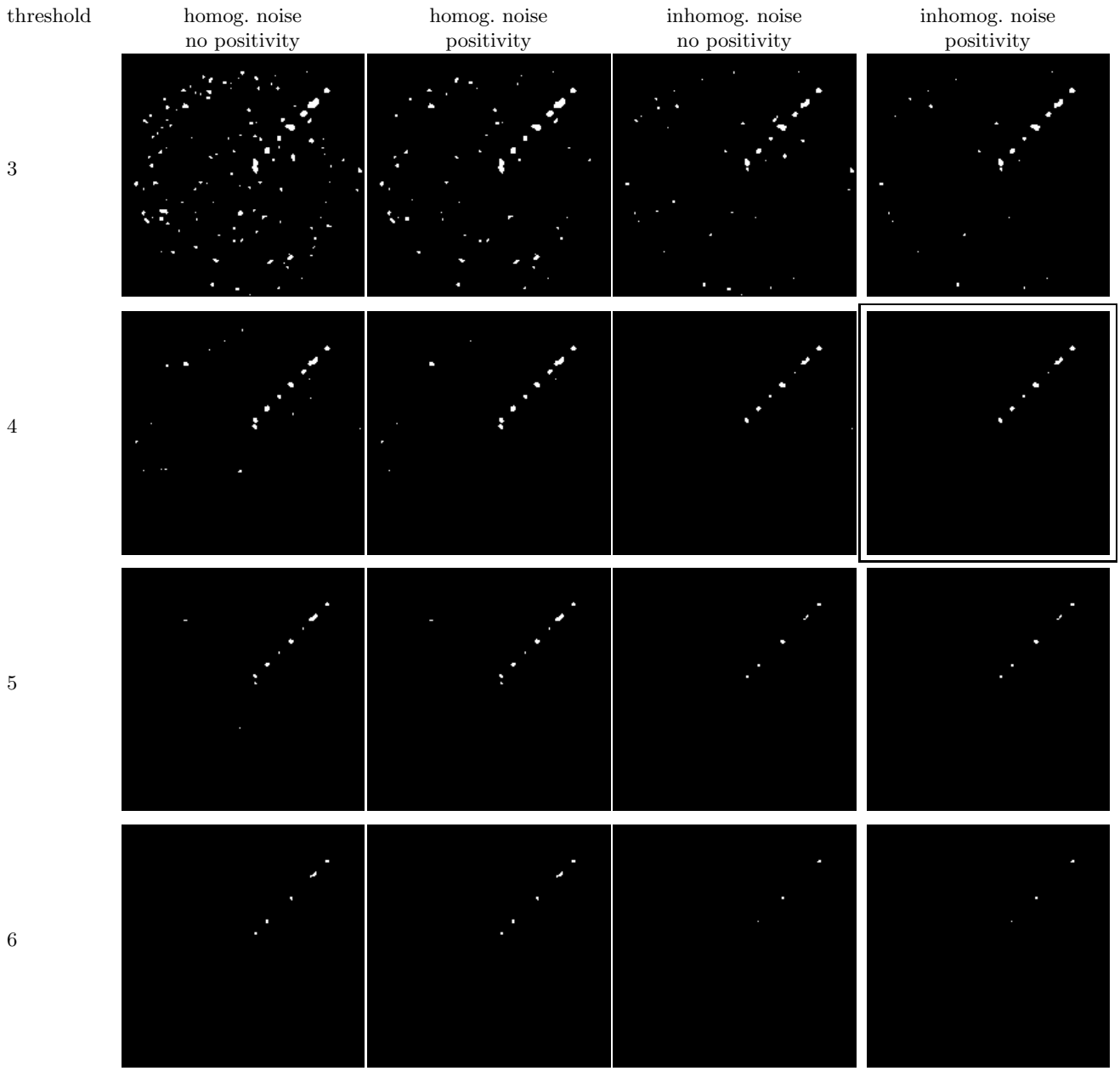

Figure 6. Detection maps obtained by thresholding the maps of the SNR of the estimated flux of Fig. 5, for various thresholds mentioned in the left column. From left to right: homogeneous noise, no positivity; homogeneous noise and positivity; inhomogeneous noise, no positivity; inhomogeneous noise and positivity.

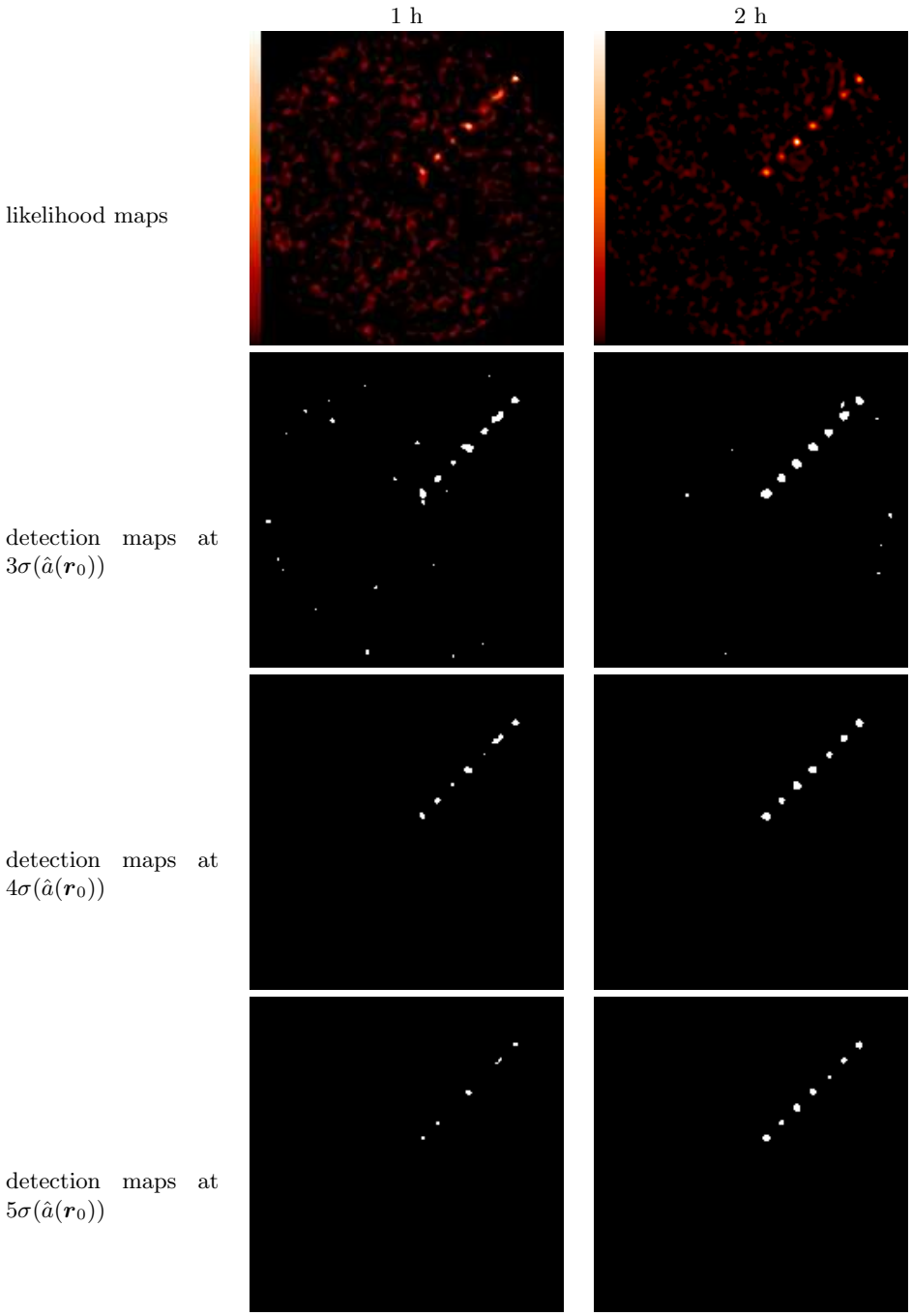

Figure 7. Likelihood and detection maps for different exposure times: 1 hour (left) and 2 hours (right), with 100 images in each case. The estimation is done with the inhomogeneous noise model and a positivity constraint.

REFERENCES

[1] J.-L. Beuzit, M. Feldt, K. Dohlen, D. Mouillet, P. Puget, J. Antici, A. Baruffolo, P. Baudoz, A. Berton, A. Boccaletti, M. Carbillet, J. Charton, R. Claudi, M. Downing, P. Feautrier, E. Fedrigo, T. Fusco, R. Gratton, N. Hubin, M. Kasper, M. Langlois, C. Moutou, L. Mugnier, J. Pragt, P. Rabou, M. Saisse, H. M. Schmid, E. Stadler, M. Turrato, S. Udry, R. Waters, and F. Wildi, "SPHERE: A 'Planet Finder' Instrument for the VLT," *The Messenger* **125**, pp. 29–+, September 2006.

[2] K. Dohlen *et al.*, "SPHERE: A planet finder instrument for the VLT," in *Ground-based and Airborne Instrumentation for Astronomy*, I. S. McLean and M. Iye, eds., **6269**, Soc. Photo-Opt. Instrum. Eng., 2006.

[3] J.-L. Beuzit, M. Feldt, K. Dohlen, D. Mouillet, P. Puget, and F. Wildi, "SPHERE: a 'planet finder' instrument for the VLT," in *Adaptive Optics Systems*, **7015**, Proc. Soc. Photo-Opt. Instrum. Eng., 2008.

[4] B. Lyot, "The study of the solar corona and prominences without eclipses (George Darwin Lecture, 1939)," *Mon. Not. R. Astr. Soc.* **99**, pp. 580–+, June 1939.

[5] D. Rouan, P. Riaud, A. Boccaletti, Y. Clénet, and A. Labeyrie, "The Four-Quadrant Phase-Mask Coronagraph. I. Principle," *Pub. Astron. Soc. Pacific* **112**, pp. 1479–1486, Nov. 2000.

[6] R. Soummer, C. Aime, and P. E. Falloon, "Stellar coronagraphy with prolate apodized circular apertures," *Astron. Astrophys.* **397**, pp. 1161–1172, Jan. 2003.

[7] K. Dohlen, M. Langlois, and M. Saisse, "The infra red dual imaging and spectrograph for SPHERE: design and performance," in *Ground-based and Airborne Instrumentation for Astronomy II*, **7014**, Proc. Soc. Photo-Opt. Instrum. Eng., 2008.

[8] A. Labeyrie, "Detection of extra-solar planets," in *Formation of Planetary Systems*, A. Brahic, ed., pp. 883–+, Cepadues-Editions, (Toulouse), 1982.

[9] C. Marois, D. Lafrenière, R. Doyon, B. Macintosh, and D. Nadeau, "Angular Differential Imaging: A Powerful High-Contrast Imaging Technique," *Astrophys. J.* **641**, pp. 556–564, Apr. 2006.

[10] I. Smith, A. Ferrari, and M. Carbillet, "Detection algorithm of exoplanets in field-rotated images: preliminary results on simulated SPHERE coronographic images," in *Semaine de l'astrophysique française*, SF2A, EDP Sciences, 2007. Conference date: July 2–6, 2007, Grenoble (France).

[11] L. M. Mugnier, J.-F. Sauvage, T. Fusco, and G. Rousset, "Multi-channel planet detection algorithm for angular differential imaging," in *Adaptive Optics: Analysis and Methods*, OSA, 2007. Conference date: June 18–20, 2007, Vancouver (Canada).

[12] J.-F. Sauvage, L. Mugnier, A. Woelfflé, T. Fusco, and G. Rousset, "Multi-channel algorithm for exoplanets detection by angular differential imaging," in *Semaine de l'astrophysique française*, J. Bouvier, A. Chalabaev, and C. Charbonnel, eds., SF2A, EDP Sciences, 2007. Conference date: July 2–6, 2007, Grenoble (France).

[13] L. M. Mugnier, T. Fusco, and J.-M. Conan, "MISTRAL: a myopic edge-preserving image restoration method, with application to astronomical adaptive-optics-corrected long-exposure images.," *J. Opt. Soc. Am. A* **21**, pp. 1841–1854, October 2004.

[14] J.-F. Sauvage, *Calibration et méthodes d'inversion en imagerie haute dynamique pour la détection directe d'exoplanètes.* PhD thesis, Université Paris VII, décembre 2007.